ELSEVIER

Inorganica Chimica Acta 334 (2002) 343–354

Inorganica Chimica Acta

www.elsevier.com/locate/ica

Ligand dependent structural changes in the acid–base chemistry of electron deficient benzoheterocycle triosmium clusters

Edward Rosenberg [a,*], Md. Joynal Abedin [a], Dalia Rokhsana [a], Alessandra Viale [b], Walter Dastru' [b], Roberto Gobetto [b], Luciano Milone [b,*], Kenneth Hardcastle [c]

[a] *Department of Chemistry, University of Montana, Missoula, MT 59812, USA*
[b] *Dipartimento di Chimica IFM, Università di Torino, via P. Giuria 7-9, 10125 Torino, Italy*
[c] *Department of Chemistry, Emory University, Atlanta, GA 30322, USA*

Received 19 October 2001; accepted 20 December 2001

Abstract

The reactions of the electron deficient benzoheterocycle clusters $Os_3(CO)_9(\mu_3\text{-}\eta^2\text{-L–H})(\mu\text{-H})$ (L = phenanthridine, **2**; 5,6-benzoquinoline, **3**; quinoxaline, **4**; 2-methyl benzimidazole, **5**; 2-methyl benzotriazole, **6**; 2-methyl benzothiazole, **7**; benzothiazole, **8**; 2-methyl benzoxazole, **9**; benzoxazole, **10**) with n-butylamine and with the protic acids HBF_4 and CF_3CO_2H are reported. Complexes **2** and **3** behave very similarly to the analogous quinoline complex (L = quinoline, **1**) forming adducts with n-butylamine with similar spectral properties to **1** and undergoing simple protonation at the metal core with both HBF_4 and CF_3CO_2H. Complexes **4**–**10** on the other hand form an additional amine adduct with different spectral characteristics than **1**–**3** and in the case of **5** this is the only detectable product. In addition, these compounds also form adducts with acetonitrile while **1**–**3** do not. Compounds **4**–**9** also exhibit much more complex behavior in the presence of CF_3CO_2H than **1**–**3**, giving trifluoroacetate adducts subsequent to initial protonation. Although **4**, **5** and **10** behave differently than **1** with n-butylamine and protic acids they form exactly the same triphenyl phosphine adduct as **1** and **3** based on multinuclear NMR data. The solid-state structure for the amine adduct of **2** is reported and suggested structures for the other amine and acid adducts, based on NMR data, are presented. The reasons for the differences in the behavior of the three distinct groups of benzoheterocycles (**1**–**3**, **4** and **5**–**10**) are discussed.

Keywords: Cluster compounds; Osmium; Heterocycles; Coordination chemistry

1. Introduction

We have been studying the chemistry of the electron deficient triosmium clusters $Os_3(CO)_9(\mu_3\text{-}\eta^2\text{-L–H})(\mu\text{-H})$ (L = quinoline, **1**; phenanthridine, **2**; 5,6-benzoquinoline, **3**; quinoxaline, **4**; 2-methyl benzimidazole, **5**; 2-methyl benzotriazole, **6**; 2-methyl benzothiazole, **7**; benzothiazole, **8**; 2-methyl benzoxazole, **9**; benzoxazole, **10**; Fig. 1) that result from the reaction of $Os_3(CO)_{10}(CH_3CN)_2$ with a wide range of benzoheterocycles (all having a pyridinyl nitrogen β- to a CH on the fused benzene ring) after photolysis of the initially formed $Os_3(CO)_{10}(\mu\text{-}\eta^2\text{-L–H})(\mu\text{-H})$ [1–8]. The solid state structures of **1**–**10** reveal that the metal–ligand bond lengths are remarkably similar throughout the series (Os–N = 2.10–2.17(2); Os–C = 2.25–2.32(2) Å) [5]. However, in our previous studies of the electrochemistry of these compounds, we found that **1**–**10** have very different electrochemical properties [8]. Thus, compound **1** exhibits two well-separated and chemically irreversible $1e^-$ reduction potentials while the first reduction potentials for **2** and **3** result in the formation of stable radical anions. Compounds **5**–**10**, on the other hand exhibit two irreversible overlapping $1e^-$ reduction potentials. The first reduction potentials correlate reasonably well with the metal–metal bond n to σ* transition in the 600–700 nm region, suggesting that they are metal based, but the wide variation in the overall electrochemical behavior of **1**–**10** suggests that ligand orbitals are important in determining the chemi-

* Corresponding authors. Tel.: +1-406-243 2592; fax: +1-406-243 4227.
E-mail address: rosen@selway.umt.edu (E. Rosenberg).

0020-1693/02/$ - see front matter
PII: S0020-1693(02)00794-6

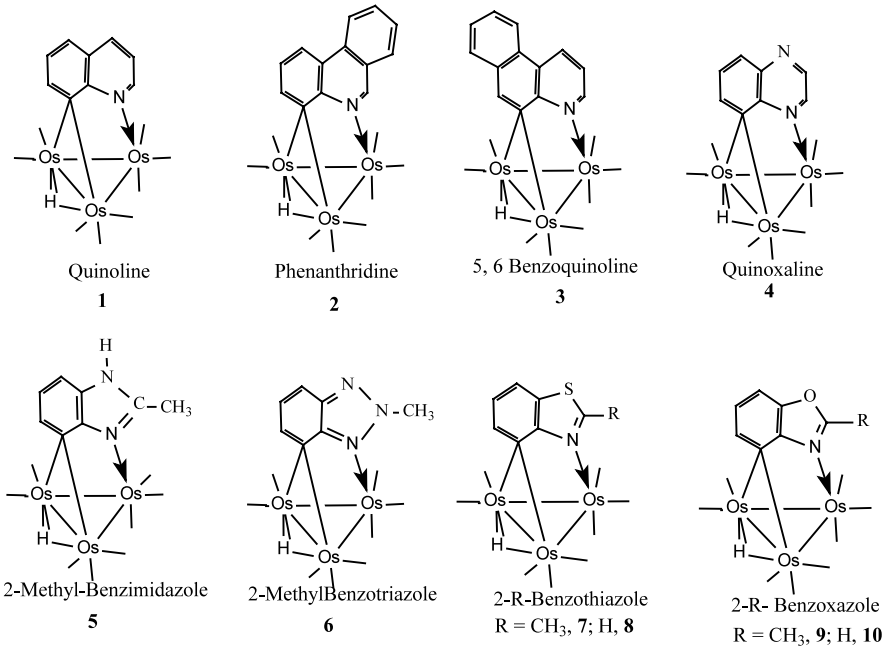

Fig. 1. Structures of compounds **1**–**10** as determined by single crystal X-ray diffraction methods.

cal behavior of these systems despite their structural similarities.

We recently completed a study of the reactions of **1** with amines and with protic acids [3]. We found that **1** was selective for primary amines and that it undergoes simple protonation at the metal core with both HBF_4 and CF_3CO_2H. The latter is known to form adducts with related heterocycle triosmium clusters [9]. We found that both the ability to coordinate amines (Lewis acid properties) and the basicity of the metal core were influenced by the nature of the substituent at the 5-position of the quinoline ring. Electron donating groups at this position enhanced the basicity of the metal core and decreased its ability to bind amines [5]. In light of these results and the electrochemical behavior of **1**–**10** discussed above, we thought it would be useful to survey the reactions of these complexes with amines and with protic acids in order to determine if the observed differences in electrochemical behavior carry over to their acid–base properties and in order to compare their reactivity with **1**. We report the results of these studies along with the related reactions of these complexes with acetonitrile and triphenylphosphine.

2. Results and discussion

2.1. Reactions with triphenylphosphine, acetonitrile and n-butylamine

The complexes **1**–**10** (Fig. 1) can be divided into three structural types: (1) those related to quinoline, **1**–**3**; (2) quinoxaline, **4**; and (3) the 6,5-fused ring systems with two or three heteroatoms, **5**–**10**. All three of these structural types react with triphenylphosphine to give the adducts $Os_3(CO)_9(\mu\text{-}\eta^2\text{-L–H})(\mu\text{-H})PPh_3$ (L = quinoline, **11**; 5,6-benzoquinoline, **12**; quinoxaline, **13**; 2-methyl benzimidazole, **14**; benzoxazole, **15**). We previously reported the structures of **11** and **12** which have the phosphine ligand in a radial position *cis*- to the hydride and residing on the carbon bound osmium atom, based on a solid state structure of **11** and the almost identical ^{13}C NMR of **11** and **12** (structure **A**, Scheme 1; Table 1) [1,2,6]. A key feature of the ^{13}C NMR of **11** and **12** is the observation of three broadened resonances attributable to the tripodal motion of three of the four carbonyl groups of the $Os(CO)_4$ moiety (resonances **g**, **h**, **i**; Table 1). At low temperatures (−40 °C) the expected *trans*-^{13}C–^{13}C coupling of 30–35 Hz is observed between the resonances assigned to

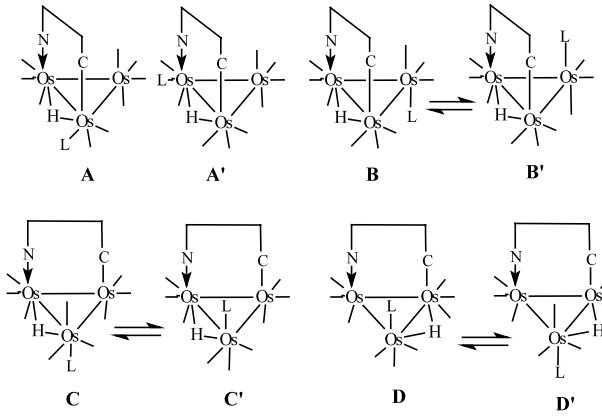

Scheme 1.

Table 1
Proton coupled ^{13}C NMR data for the phosphine adducts of the electron deficient benzoheterocycle complexes [a]

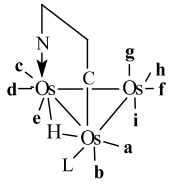

A

Ring	No.	a	b	c	d	e	f	g	h	i
Quinoline[b]	**11**	182.53(dd) J_{CH}=7.5 J_{PC}=4.5	185.73(d) J_{PC}=6.1	177.95(d) J_{CH}=13.7	177.68(d) J_{CH}=3.1	177.87(d) J_{CH}<1	176.54(s)	184.52(s)	178.03(s)	184.22(s)
5,6 Benzo quinoline[c]	**12**	182.53(dd) J_{CH}=9.0 J_{PC}=4.6	185.64(d) J_{PC}=6.2	178.10(d) J_{CH}=13.0	177.93(d) J_{CH}=4.5	177.06(s)	176.50(s)	184.50(s)	178.02(s)	184.43(s)
Quinoxaline	**13**	182.77(dd) J_{CH}=8.0 J_{PC}=4.6	187.04(d) J_{PC}=6.1	177.82(d) J_{CH}=14.0	178.14[d](d)	178.19(s)	177.15(s)	185.72(s)	178.72(s)	185.82(s)
2-Me-Benzimidazole	**14**	184.04(dd) J_{CH}=11.0 J_{PC}=5.0	188.24(d) J_{PC}=6.0	177.90(d) J_{CH}=13.0	176.76(d) J_{CH}=3.0	179.25(d) J_{CH}=1	178.59(s)	186.41(s)	178.59(s)	185.17(s)
Benzoxazole	**15**	184.18[d] J_{PC}=6.0	186.53(d) J_{PC}=6.0	174.10(d) J_{CH}=13.7	173.15(d) J_{CH}=3.0	177.52(s)	175.60(s)	184.27(s)	176.60(s)	182.14(s)

[a] Chemical shifts are in ppm downfield relative to TMS, coupling constants in Hz at 25 °C. [b] From Ref. [1]. [c] From Ref. [6]. [d] J_{CH} not observed due to overlap of resonances.

carbonyls **g** and **i** confirming the presence of the $Os(CO)_4$ group. The ^{13}C NMR spectra of compounds **13**–**15** also exhibit these features and indeed have ^{13}C NMR spectra that are very similar to **11** and **12** (Table 1). On this basis we assign structure **A** to all of these phosphine adducts (Scheme 1). In the case of benzoxazole, a second minor isomer is observed as evidenced by the observation of a second doublet in the hydride region at −16.14 ($J^{31}P-^{1}H = 14.2$ Hz) along with companion peaks to the major isomer in the ^{1}H and ^{13}C NMR. Although overlap of resonances and the inseparability of the two isomers precluded the characterization of this minor product we suggest that it has the phosphine substituent on the nitrogen bound osmium atom (structure **A′**, Scheme 1) as has been previously reported for related nitrogen heterocycle triosmium complexes [11].

We have previously reported that **1** and its substituted derivatives undergo ligand cleavage in acetonitrile at 70–80 °C in the presence of 1 atm of CO to yield $Os_3(CO)_{12}$ and the free quinoline [4,5]. It seems reasonable to suggest that the first step in this process is the formation of an acetonitrile adduct. However, compounds **1**–**3** shows no evidence for adduct formation when dissolved in acetonitrile, maintaining their green color and exhibiting only minor shift changes in their ^{1}H NMR. In sharp contrast, compounds **5** and **10** undergo an immediate color change, from dark to light green and dark green to yellow, respectively, on dissolution in acetonitrile and show significant changes in their ^{1}H and ^{13}C NMR relative to $CDCl_3$ (Tables 2 and 3). In the case of **5**, the light green solution shows evidence for the presence of residual starting material in its ^{1}H NMR as well as the presence of two new hydride resonances at −12.15 and −12.40 ppm and associated new aromatic and NH resonances. The hydride resonances of the two new species present integrate in a ratio of 11.6:1 with the hydride resonance attributable to **5**. Using the starting moles of **5** in the solution, the volume of acetonitrile and the hydride integration ratios we can estimate the equilibrium constant for the reaction of **5** with acetonitrile to be 0.68 M^{-1}. The main feature of the proton coupled ^{13}C NMR in the carbonyl region is the observation of two closely spaced doublets ($\Delta\delta = 1.4$) with relatively large coupling to the bridging hydride (Table 3). This feature is also observed in the decacarbonyl of **10** where $\Delta\delta = 1.4$ (Table 3). This small value for the $\Delta\delta$ of the carbonyls *trans*- to the hydride is indicative of a structure where the benzoheterocycle bridges the same edge as the hydride and the acetonitrile is coordinated to the unbridged osmium (structure **B**, Scheme 1). This same feature was also observed for the acetonitrile adduct of the imidoyl complex $Os_3(CO)_9(\mu_3\text{-}\eta^2\text{-}(CH_2)_3C{=}N{-})(\mu\text{-H})$, where a crystal structure was obtained ($\Delta\delta = 0.05$) [10]. The assignments given in Table 3 for the carbonyl groups of the acetonitrile adducts of **4**, **5** and **10** were made on the basis of established trends in chemical shift and coupling constant data for these types of cluster [3,10]. These assignments are by no means unambiguous but the

Table 2
^{1}H NMR of acetonitrile adducts of electron deficient benzoheterocycle clusters [a]

Ring	No	Solvent	H(2)	H(3)	H(4)	H(5)	H(6)	H(7)	2-Me	NH	Hydride
Quioxaline	**4**[b]	$CDCl_3$	9.15(d)	8.54(d)		8.67(dd)	7.46(dd)	8.72(dd)			-12.16(s)
Quinoxaline	**4**	CD_3CN	9.49(d)	8.49(d)		8.61(dd)	7.36(dd)	8.53(dd)			-11.24(s)
2-Me Benzimidazole	**5**[b]	$CDCl_3$			6.98(dd)	8.16(m)	8.16(m)		2.75(s)	.9.02(s,br)	-11.78(s)
2-Me Benzimidazole	**5**	CD_3CN			7.54(d)	6.80(m)	6.80(m)		2.65(s)	7.66(br)	-12.15(s) -12.40(s)[c]
Benzoxazole	**10**	$CDCl_3$	8.29(s)		8.46(d)	7.26(dd)	8.50(d)				-11.84(s)
Benzoxazole	**10**	CD_3CN	8.69(s)		7.03(m)	6.95(m)	7.64(d)				-12.52(s)

[a] Chemical shifts are in ppm downfield positive relative to TMS 25 °C.
[b] From Ref. [5].
[c] Minor isomer.

Table 3
Proton coupled ^{13}C NMR of the acetonitrile adducts of the electron deficient benzoheterocycle complexes [a]

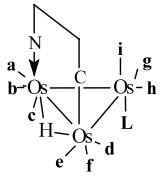

B

Ring	No	L	a	b	c	d	e	f	g	h	i
Quinoxaline[c]	**4**	CD_3CN	181.82(d) J_{CH}=12.1	182.34(d) J_{CH}=4.0	179.69(s)	180.91(d) J_{CH}=9.1	183.01(d) J_{CH}=2.5	182.60(s)	182.61(s)	183.94(s)	185.57(s)
2-Me-Benzimidazole	**5**	CD_3CN	182.00(d) J_{CH}=11.1	182.19(d) J_{CH}=3.7	180.64(s)	180.64(d) J_{CH}=8.3	181.15(d) J_{CH}=3.7	183.84(s)	183.13(s)	183.02(s)	185.04(s)
Benzoxazole	**10**	CD_3CN	177.71(d) J_{CH}=12.0	178.03(d) J_{CH}=2.7	179.72(s)	179.11(d) J_{CH}=8.5	179.72(d) J_{CH}=2.0	181.90(s)	181.83(s)	182.94(s)	183.58(s)
Benzoxazole	**16**	CO	173.19(d) J_{CH}=12.3	172.96(d) J_{CH}=3.8	176.17(s)	173.97(d) J_{CH}=8.5	175.16(d) J_{CH}=3.0	177.95(s)	174.59(s)	175.639s)	182.88 (183.13)[b]

[a] Chemical shifts are downfield positive relative to TMS in ppm and coupling constants are given in Hz at 25 °C. [b] Two axial carbonyls are observed with the expected ^{13}C–^{13}C satellites. [c] Major isomer only.

general features as discussed above allow us to distinguish between the structural isomers possible (vide infra). We cannot, of course, differentiate between structures **B** and **B′** (Scheme 1) based on the current data; **B** is chosen here based on analogy with previously reported acetonitrile adducts [10]. Further evidence that the structures of the decacarbonyl and acetonitrile adduct of **5** are the same comes from the fact that they both have the similar T_1 values for the hydride in acetonitrile (7.2 and 8.0 s, respectively). Compound **4** undergoes a color change from dark green to red (the same color as the decacarbonyl), and the ^{1}H and ^{13}C NMR data support formation of an acetonitrile adduct with structure **B** or **B′** (Tables 2 and 3). In addition to one major adduct isomer and residual starting material solutions of **4** in acetonitrile show the presence of three minor isomers. One of the minor isomers shows a set of sharp resonances partially overlapping with the major isomer and a hydride resonance at −11.04 ppm and can tentatively be assigned to **B′** [10]. The two other isomers show broad hydride resonances at −13.61 and −13.85 ppm in a relative intensity of 10:1 with companion broad resonances in the aromatic region. The broadness of these lines and the chemical shifts of the hydrides suggest the population of isomers such as **C/C′** or **D/D′** (Scheme 1, vide infra). This was not the case for **5** or **10**.

It is important to note here that although **4**–**10** form adducts with acetonitrile while **1**–**3** do not, the rings are not cleaved from the cluster at any significant rate when heated in this solvent at 70–80 °C under 1 atm of CO as are **1**–**3**. This seems contradictory unless one considers the possibility that cleavage of the ligand is controlled thermodynamically by the relative stability of the μ_3 and μ bonding modes for **1**–**3** versus **4**–**10** (Fig. 2 represents a qualitative picture of the situation). The reasons why the μ-bonding mode should be more stable thermodynamically for **4**–**10** than the μ_3-compared with **1**–**3** are not apparent and must await a theoretical treatment of the bonding in these systems. It is clear that all the μ_3-complexes are kinetically stable and that adduct forma-

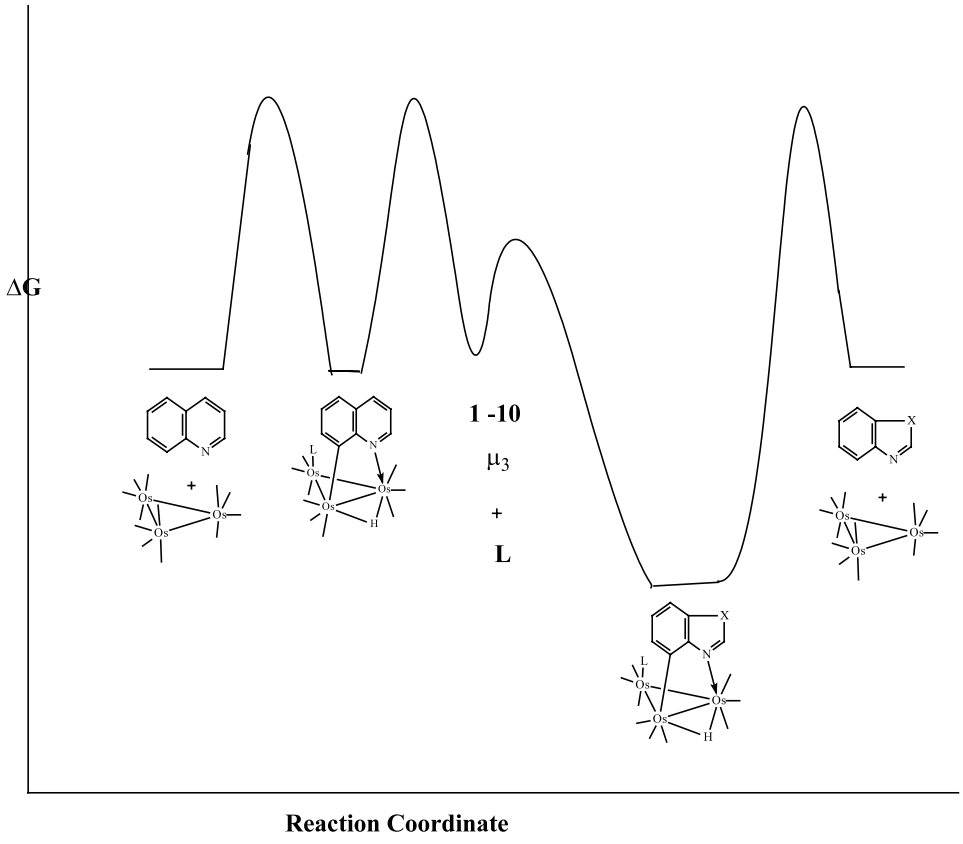

Fig. 2. Reaction profile diagram for ligand coordination and cleavage, illustrating the proposed difference in the relative stability of the μ- and μ_3-bonding modes for **1**–**10**.

tion must precede ligand cleavage because cleavage of **1**–**3** does not proceed in solvents other than acetonitrile.

Compounds **1**–**10** all react with n-butylamine to form yellow adducts, but here again there are significant differences between the different structural types. In our previous studies with **1**, we suggested the isomeric structures **C** and **C′** for the amine adducts with **C** being the major isomer based on solution NMR data, T_1 measurements and by analogy with related structurally characterized ammonia adducts [10]. Compounds **2**–**4** appear to form the same two isomers but in the case of **2** and **3** the adducts precipitated from chloroform necessitating measurement of the isomer ratios and equilibrium constants in acetone (Table 6). As for **1**, we observe the formation of a single isomer and then the gradual appearance of a second isomer. We previously showed that this process involves formation of an isomer with the amine ligand on the same face of the cluster as the heterocycle followed by an intermolecular equilibration to a mixture of isomers with the amine ligand on either face of the metal triangle.

In the case of **2**, we were able to isolate crystals of the amine adduct, $Os_3(CO)_9(\mu_3\text{-}\eta^2\text{-L–H})(\mu\text{-H})(\text{n-}C_4H_9N)$ (L = phenanthridine, **16**), suitable for a solid-state structural investigation. The solid-state structure of **16** is shown in Fig. 3, crystal data are given in Table 4 and selected distances and bond angles in Table 5. The solid-state structure of **16** reveals that the hydride and the benzoheterocycle bridge different edges of the cluster, with the amine ligand and the phenanthridine ring on the same face of the cluster. The hydride bridges the osmium atom coordinated to the amine and the osmium atom bound to C(8) (quinoline numbering system) of the phenanthridine ring. The overall structure is represented by structure **D** (Scheme 1). In light of the very similar spectroscopic properties of **1**–**3**, we must revise our earlier assignment of the amine adduct of **1** to structure **C** and assign the solution structures of all three amine adducts to an equilibrium mixture of **D** and **D′**. The hydride was located along the longest edge of the metal triangle (Os(1)–Os(2) = 3.0405(6) Å) using the program HYDEX [12]. The phenanthridine ligand bridges the second longest edge of the metal triangle (Os(2)–Os(3) = 2.8873(6) Å) while the unbridged edge has the shortest metal–metal bond distance (Os(1)–Os(3) = 2.7810(5) Å). The metal nitrogen bond distances are essentially equal (Os(2)–N(1S) = 2.209(7) and Os(3)–N(1B) = 2.195(7) Å and are approximately the same as the metal carbon bond distance with the phenanthridine ligand (Os(1)–C(12B) = 2.190(9) Å). These distances are some longer than related distances in $Os_3(CO)_9(\mu\text{-}\eta^2\text{-L–H})(\mu\text{-H})(L')$ complexes [2,5]. The n-butylamine ligand

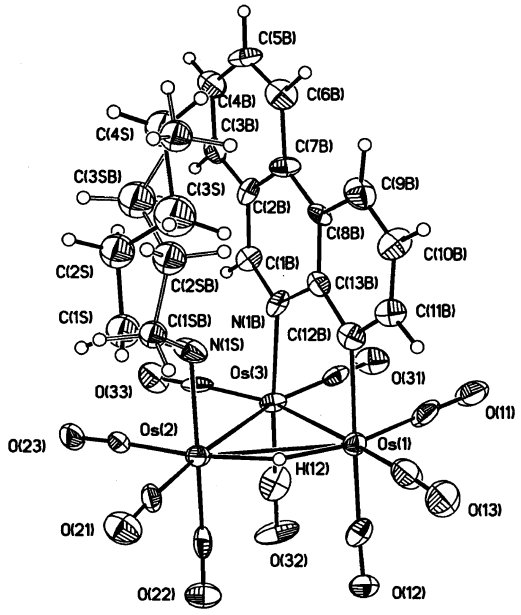

Fig. 3. Solid state structure of $Os_3(CO)_9(\mu\text{-}\eta^2\text{-L}–H)(\mu\text{-H})(n\text{-}C_4H_9N)$ (L = phenanthridine, **16**).

Table 4
Crystal data and structure refinement for **16**

Empirical formula	$C_{26}H_{20}N_2O_9Os_3$
Formula weight	1073.02
Temperature (K)	100(2)
Wavelength (Å)	0.71073
Crystal system	monoclinic
Space group	$P2(1)/n$
Unit cell dimensions	
a (Å)	9.0881(8)
b (Å)	21.789(2)
c (Å)	13.9362(13)
α (°)	90
β (°)	99.771(2)
γ (°)	90
V (Å^3)	2719.6(4)
Z	4
D_{calc} (mg m^{-3})	2.621
Absorption coefficient (mm^{-1})	14.038
$F(000)$	1952
Crystal size (mm^3)	0.14 × 0.05 × 0.04
θ Range for data collection (°)	1.75–32.86
Index ranges	$-13 \le h \le 13$, $-33 \le k \le 32$, $-20 \le l \le 20$
Reflections collected	34 853
Independent reflections	9576 [$R_{int} = 0.1256$]
Completeness to $\theta = 32.86°$	94.5%
Absorption correction	SADABS2
Max/min transmission	1.00000 and 0.721709
Refinement method	Full-matrix least-squares on F^2
Data/restraints/parameters	9576/0/357
Final R indices [$I > 2\sigma(I)$]	$R_1 = 0.0589$, $wR_2 = 0.0656$
R indices (all data)	$R_1 = 0.1343$, $wR_2 = 0.0734$
Goodness-of-fit on F^2	1.081
Largest difference peak and hole (e Å^{-3})	2.396 and −2.492

Table 5
Selected distances (Å) and bond angles (°) for $Os_3(CO)_9(\mu_3\text{-}\eta^2\text{-L}–H)(\mu\text{-H})(n\text{-}C_4H_9N)$ (L = phenanthridine, **16**)

Bond distances			
Os(1)–Os(2)	3.0405(6)	N(1S)–C(1S)	1.50(1)
Os(1)–Os(3)	2.7810(5)	N(1B)–C(1B)	1.297(9)
Os(2)–Os(3)	2.8873(6)	N(1B)–C(13B)	1.46(1)
Os(1)–C(12B)	2.190(9)	C(1B)–C(2B)	1.41(1)
Os(2)–N(1S)	2.209(7)	C(11B)–C(12B)	1.40(1)
Os(3)–N(1B)	2.195(7)	C(12B)–C(13B)	1.43(1)
Os–CO [a]	1.89(1)		
Bond angles			
Os(1)–Os(2)–Os(3)	55.88(1)	C(1S)–N(1S)–Os(2)	117.1(8)
Os(1)–Os(3)–Os(2)	64.85(1)	C(1B)–N(1B)–Os(3)	118.2(8)
Os(2)–Os(1)–Os(3)	59.27(1)	C(13B)–N(1B)–Os(3)	123.0(5)
Os(1)–Os(2)–N(1S)	89.7(2)	C(13B)–C(12B)–Os(1)	125.4(7)
Os(3)–Os(2)–N(1S)	89.1(2)	C(11B)–C(12B)–Os(1)	119.9(7)
Os(1)–Os(3)–N(1B)	86.8(1)	C(1B)–N(1B)–C(13B)	118.2(8)
Os(2)–Os(3)–N(1B)	92.7(1)	C(11B)–C(12B)–C(13B)	114.4(9)
Os(2)–Os(1)–C(12B)	91.3(2)		
Os(3)–Os(1)–C(12B)	85.6(2)		
Os–C–O [a]	176.4(9)		

Numbers in parentheses are average standard deviations.
[a] Average values.

and the phenanthridine ligand are perpendicular to the plane of the metal triangle as can be seen from the Os–Os–N(1B), Os–Os–N(1S) and Os–Os–C(12B) angles (Table 5). The n-butylamine ligand is disordered, axially with a conformational population of 0.59:0.41 (Fig. 3).

The formation constants for **1**–**3** evaluated after isomer equilibration are quite similar as are the **D**/**D′** isomer ratios and the hydride chemical shifts (Table 6). This might be expected for these very similar heterocycles. The ^{13}C NMR patterns for the amine adducts of **1** and **2** are very similar and the T_1's of the hydrides are almost identical and are significantly shorter than for **1** and **2** (4.0 and 5.2 s for **1** and **2**, respectively; Tables 6 and 7). The short T_1 values for these adducts are attributable to enhanced dipolar relaxation indicative of the close proximity of the amine to the hydride ligand. In the ^{13}C NMR of the carbonyl region of ^{13}CO enriched samples of the amine adducts of **1** and **2** no ^{13}C–^{13}C coupling satellites are observed. Based on this evidence it is reasonable to propose the n-butylamine adducts of **1**–**3** exist in solution as the same set of isomers, **D** and **D′**.

Compounds **4**–**10** all show an increase in their formation constants with n-butylamine relative to **1**–**3** while the **D**/**D′** ratio remains about the same as in **1**–**3** with the exception of **4**. This increase in the formation constant is consistent with the fact that **4**–**10** form acetonitrile adducts while **1**–**3** do not. In addition, the appearance of a third new hydride resonance is observed at slightly lower fields (−11–12 ppm) for **5**–**10** (Table 6). In the case of **5**, this is the only adduct hydride resonance observed and therefore allowed us to examine the structure of this isomer in detail. The ^{13}C NMR of

Table 6
^{1}H NMR, isomer ratios, hydride T_1 and formation constants for n-butylamine adducts of electron defiicient benzoheterocycle clusters [a]

Ring	No.	Solvent	δ(**D**)	δ(**D′**)	δ(**C**)	K(**D**/**D′**)	**C**/**D**+**D′**	Hydride T_1	K_{form} (M^{-1}) [c]
Quinoline	**1**	$CDCl_3$	−13.39	−12.76		2.8		1.4	44.4
Phenanthridine	**2**	$(CD_3)_2CO$	−13.23	−12.56		2.2		1.5	18.3
5,6-Benzoquinoline	**3**	$(CD_3)_2CO$	−13.33	−12.73					
Quinoxaline	**4**	$CDCl_3$	−13.55	−13.05		0.66			303
2-Me-benzimidazole	**5**	CD_2Cl_2			−11.78			5.2, 6.9 (15.2) [b]	124
2-Me-benzotriazole	**6**	$CDCl_3$	−13.67	−13.15	−11.67	1.56	0.69		232
2-Me-benzothiazole	**7**	$CDCl_3$	−13.46	−12.86	−11.07	2.59	1.61		47
Benzothiazole	**8**	CD_2Cl_2	−13.52	−12.98	−11.46	2.54	0.23		274
2-Me-benzoxazole	**9**	$CDCl_3$	−13.60	−13.06	−11.86	2.0	2.0		310
Benzoxazole	**10**	CD_2Cl_2	−13.63	−13.15	−12.09	1.09	0.51		1097

[a] Chemical shifts in ppm downfield positive from TMS 25 °C. [b] T_1 for NH_3 complex (ND_3 complex). [c] Calculated using the relative intensity of the hydride resonances of all observed isomers, the moles of starting complex and the amount of amine added.

Table 7
^{13}C NMR data for amine adducts of the electron deficient benzoheterocycle complexes [a]

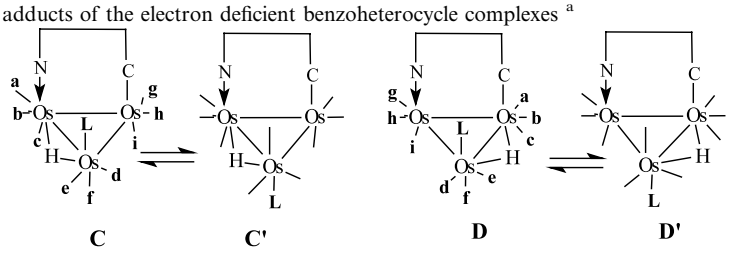

Ring	No	a	b	c	d	e	f	g	h	i
Quinoline-[b] Structure **D**	**1**	178.8(d) JCH=14.0	180.4(s)	186.5(s)	177.3(d) JCH=9.0	179.8(s)	187.3(s)	176.7(s)	176.2(s)	185.5(s)
Phenanhridine[c] Structure **D**	**2**	179.26(d) JCH=12.3	181.37(d) JCH=3.8	188.54(s)	178.93(d) JCH=9.2	178.44(d) JCH=1.0	185.26(s)	181.36(s)	180.51(s)	184.48(s)
Benzimidazole Structure -**C**	**5**	179.2(d) JCH=9.2	180.67(d) JCH=3.1	182.53(s)	183.77(d) JCH=10.8.	181.66(d) JCH=3.8	186.65(s)	177.26(s)	179.96(s)	186.12(s)

[a] Chemical shifts in ppm downfield positive relative to TMS 25 °C. [b] From Ref. [3], L = NH_3. [c] L = n-$BuNH_2$.

this adduct has a distinctly different pattern than that observed for **D** in **1**–**3** with the carbonyl resonances *trans*- to the hydride being much more well separated ($\Delta\delta = 4.6$) suggesting that the two hydride bridged osmium atoms are in a different environment than in **D**. The T_1 of the n-butylamine adduct of **5** is 5.2 s which is considerably shorter than the T_1 of the decacarbonyl of **5** (11.5 s) that has structure **B**. The T_1's of **1**–**3** and their amine adducts are, on the other hand, considerably shorter and so we decided to evaluate the T_1 values for the NH_3 and ND_3 adducts of **5** in order to get a more definitive idea of the proximity of the amine hydrogens to the hydride. The values obtained of 6.9 and 15.2 s for the NH_3 and ND_3 adducts, respectively, clearly indicate that the amine ligand resides on an osmium atom bound to the bridging hydride. Taken together with the ^{13}C NMR data, we suggest structure **C** or **C′** for the amine adduct of **5**. That the T_1 values of **5**, the decacarbonyl of **5** and its amine adduct are all longer than the corresponding values for **1** probably reflects the replacement of the hydrogen at C(2) with a methyl group. In the case of **10**, a fourth hydride resonance is observed at −11.26 ppm very close the resonance we have assigned to **C** or **C′** in a relative intensity of 1:1.2. It would appear that both **C** and **C′** are populated in this case and this isomer was included in the calculation of the formation constant for the amine adduct of **10** (Table 6). That isomers **C** and/or **C′** are preferred for **5** and populated for **5**–**10** may attributed to contributions that make the pyridinyl nitrogen more basic and therefore favor the isomer where the acidic hydride bridges the edge of the metal triangle to which both basic nitrogens are bound (Scheme 2). In the case of the amine adduct of **5** we were able to isolate analytically pure samples of the n-butylamine adduct $Os_3(CO)_9(\mu\text{-}\eta^2\text{-L–H})(\mu\text{-H})(n\text{-}C_4H_9N)$ (L = 2-me-benzimidazole, **17**) these crystals

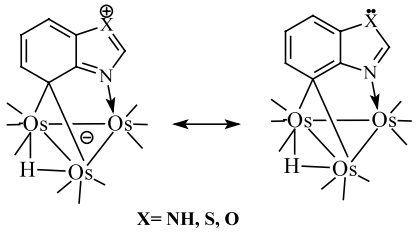

Scheme 2.

were not suitable for solid-state structural analysis but do corroborate the formulation of the adducts with the proposed structure **C**.

Table 8
Hydride chemical shifts for initial protonation products of the electron deficient benzohetrocycle complexes [a]

Ring	No.	δ(hydride)	δ(hydride)	Acid
Quinoline	**1**	−13.70(d) (1.6)	−11.65(d)	HBF_4
Quinoline	**1**	−13.66(d) (1.7)	−11.61(d)	CF_3CO_2H
Phenanthridine	**2**	−13.71(d) (1.6)	−11.73(d)	HBF_4
Phenanthridine	**2**	−13.70(d) (1.7)	−11.73(d)	CF_3CO_2H
5,6-Benzoquinoline	**3**	−14.08(d) (1.6)	−11.74(d)	HBF_4
5,6-Benzoquinoline	**3**	−14.10(d) (1.6)	−11.73(d)	CF_3CO_2H
Quinoxaline	**4**	−13.71(d) (1.6)	−11.63(d)	HBF_4
2-Me-benzimidazole	**5**	−13.36(d) (1.7)	−12.61(d)	HBF_4
2-Me-benzotriazole	**6**	−13.22(d) (1.6)	−11.98(d)	HBF_4
2-Me-benzothiazole	**7**	−13.50(d) (1.4)	−12.42(d)	HBF_4
Benzothiazole	**8**	−13.41(d) (1.2)	−12.24(d)	HBF_4
2-Me-benzoxazole	**9**	−13.43(d) (1.4)	−12.61(d)	HBF_4
Benzoxazole	**10**	−13.38 (s)	−12.66 (s)	HBF_4

[a] Chemical shifts in ppm downfield positive from TMS; numbers in parenthesis are coupling constants between the hydrides in Hz at 25 °C.

2.2. Reactions with HBF_4 and CF_3CO_2H

Compounds **1**–**3** undergo simple protonation with HBF_4 and CF_3CO_2H as evidenced from their ^1H and ^{13}C NMR (Tables 8 and 9). The solutions go from dark green to orange on addition of both acids and the resulting ^1H and ^{13}C NMR spectra are virtually identical and can be assigned to structure **E** (Scheme 3) [3]. Compounds **4**–**10** also protonate with HBF_4 but with CF_3CO_2H yellow solutions are formed and the ^1H, ^{13}C and ^{19}F spectra give strong evidence for the formation of trifluoroacetate adducts (Scheme 3), consistent with the greater tendency of these compounds to form adducts with Lewis bases as described above [9]. The changes in the spectra of **4**–**10** vary from compound to compound and will be discussed individually below. In the case of **4**–**10**, we observed no evidence of protonation of the heteroatoms and this is particularly surprising in the case of **4** but consistent with the decreased basicity of the uncoordinated lone pair and the enhanced basicity of the metal core in this complex.

Addition of a twofold excess of CF_3COOH to a CD_2Cl_2 solution of **4** results in an instantaneous color change from green to orange–yellow. The hydride region of the ^1H NMR consists of two broad resonances at −12.24 and −14.08 ppm along with a small amount of starting material at −12.33 ppm. As the temperature is lowered to −50 °C these resonances sharpen and are resolved into two sets of hydrides at −12.10 and −13.78 ppm and −12.38 and −14.88 ppm, in a relative intensity of 1:2. This behavior can be understood in terms of the averaging of two isomeric adducts **F** and **F′**

Table 9
Proton coupled ^{13}C NMR of the protonated electron deficient benzoheterocycle complexes [a]

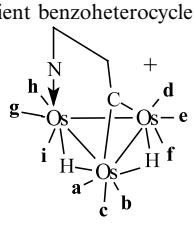

E

Ring	No	a	b	c	d	e	f	g	h	i
Quinoline[b]	**1**	159.99(dd) J_{CH}=13.7 J_{CH}=6.1	159.84(dd) J_{CH}=13.7 JCH=4.6	172.36(s)	172.45(d) J_{CH}=7.6	168.13(s)	172.92(s)	166.71(s)	180.65(d) J_{CH}=9.2	178.78(s)
Quinoxaline	**4**	161.51(dd) J_{CH}=13.7 J_{CH}<1	160.96(dd) J_{CH}=12.7 J_{CH}<1	173.69(s)	173.22(d) J_{CH}=9.1	169.42(s)	174.81(s)	168.20(s)	181.86(d) J_{CH}=9.0	181.46(s)
2-Me Benzimidazole	**5**	159.85(dd) J_{CH}=13.8 JCH=1	158.53(dd) J_{CH}=10.8 J_{CH}=1	171.74(s)	171.95(d) J_{CH}=7.7	167.82(s)	173.29(s)	167.82(s)	180.14(d) J_{CH}=9.2	175.66(s)
Benzoxazole	**10**	160.70(dd) J_{CH}=12.8 J_{CH}<1	159.08(dd) J_{CH}=13.7 J_{CH}<1	171.66(s)	172.99(d) J_{CH}=8.4	169.28(s)	173.87(s)	167.66(s)	178.62(d) J_{CH}=9.1	175.68(s)

[a] Chemical shifts are downfield positive relative to TMS in ppm and coupling constants are given in Hz at 25 °C. [b] Data from Ref. [3].

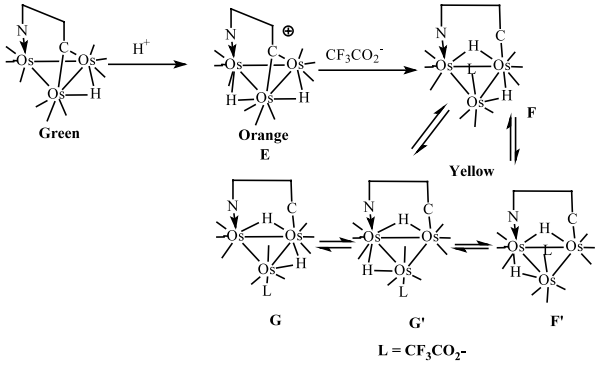

Scheme 3.

by hydride exchange. This is supported by the observation of two ^{19}F NMR resonances at 1.81 and 0.66 ppm relative to free CF_3COOH at −50 °C, in the same relative intensity as the two sets of hydride resonances, which average with each other but not with the free acid as the temperature is increased. This behavior is very similar to that observed for the related imidoyl adduct, $Os_3(CO)_9(\mu\text{-}\eta^2\text{-}(CH_2)_3C{=}N{-})(\mu\text{-}H)_2(CF_3COO)$ that has a solid state structure analogous to **F** [9].

Compound **5** undergoes only simple protonation with CF_3COOH as evidenced by the observation of two sharp hydride resonances of equal intensity at −12.63 and −13.38 ppm. These shifts are almost identical to those observed on reaction of **5** with HBF_4 and the ^{19}F NMR spectrum shows only free trifluoroacetate ion.

The behavior of **6** with CF_3COOH is distinctly different than that of **4**. Addition of 1 equiv. of this acid results in the appearance of two broad hydride resonances at −13.51 and −13.92 ppm of equal relative intensity with about 50% of the starting material remaining as a sharp resonance at −11.92 ppm. On standing overnight the relative intensity of the starting material diminishes and the two broad resonances sharpen and shift to −13.04 and −13.92 ppm. The ^{19}F NMR initially shows a somewhat broadened free trifluoroacetate peak and a broad peak at 1.68 ppm that sharpens and shifts to 1.95 ppm. Addition of a fivefold excess of acid to the solution leads only to the disappearance of the starting material and a slight further shift of the hydride signals. The ^{19}F NMR shows free trifluoroacetate and a sharp signal at 1.95 ppm in the presence of excess acid. These data are best understood in terms of formation of a adduct with structure **F** or **F′** where formation of the adduct is slow on the NMR time scale, followed by isomerization to **G** or **G′** by an intermolecular (dissociative) process in the intermediate exchange regime (Scheme 3). Apparently, only one of the two possible isomers **G** or **G′** is populated and the hydrides are fluxional at ambient temperature.

Compound **7** like **5** undergoes simple protonation with CF_3COOH as evidenced by the appearance of two sharp hydride resonances at −12.52 and −13.45 ppm, again almost identical to the hydrides observed with HBF_4. As for **5**, the ^{19}F NMR shows only free trifluoroacetate–triflouroacetic acid. Based on our observations so far it appears that adduct formation is associated with the introduction of hydride fluxionality while simple protonation results in rigid dihydride species. This behavior is reminiscent of the addition of phosphine to the rigid trihydride $Os_3(CO)_8(\mu_3\text{-}\eta^2\text{-}(CH_2)_3C{=}N{-})(\mu\text{-}H)_3$ where conversion of a μ_3-capping ligand to a μ-edge bridging mode results in inducing a high degree of fluxionality to the hydride ligands [13].

The behavior of **8** in the presence of 1 equiv. of CF_3COOH is a composite of **4** and **6**. At ambient temperature a series of broad resonances is observed but on lowering the temperature to −60 °C three pairs of hydride resonances can be seen at −13.29 and −13.68 ppm, −12.79 and −14.71 ppm and −12.85 and −13.70 ppm. A sharp peak is observed at −11.78 ppm attributable to unreacted **8**. At −90 °C these resonances shift somewhat and overlap but become sharper. On standing the pair of resonances at −12.85 and −13.70 ppm increases in intensity and finally becomes the dominant species present in solution. This behavior is paralleled in the ^{19}F NMR where three resonances at 2.15, 2.31 and 2.34 ppm are initially observed at −90 °C in addition to free trifluoroacetate at 0.0 ppm. On standing overnight the resonance at 2.15 ppm increases while the other two resonances disappear and the trifluoroacetate peak diminishes in intensity. These data can be understood in terms of initial formation of **F** and **F′** which undergo interconversion by hydride edge hopping on the NMR time scale followed by gradual conversion to either **G** or **G′** (Scheme 3).

The reaction of **9** with CF_3COOH takes a similar course but with some slight differences. As for **8** addition of 1 equiv. of CF_3COOH leads to the formation of a dihydride species with broad resonances at −13.58 and −13.99 ppm that gradually convert to a second broadened set of hydride signals on standing overnight at −13.60 and −13.88 ppm. In contrast to **8** however, this latter set of hydrides is resolved into two sets of hydrides at −13.35 and −13.83 ppm and −13.72 and −13.90 ppm in a ratio of 3:4 on lowering the temperature to −90 °C. This behavior is paralleled in the ^{19}F NMR where an initial peak at 1.75 ppm gradually converts to a peak at 2.25 ppm on standing at room temperature. Additionally, we were able to observe two sharp doublets in the hydride region of the ^{1}H NMR at −12.61 and −13.43 ppm that we assign to the presence of $\mathbf{9H}^+$. Thus the formation of **F** and **F′** is followed by conversion to **G** and **G′** where hydride edge hopping is in the fast exchange regime for both sets of isomers but where conversion of **F** to **G** is slow. That $\mathbf{9H}^+$ can be detected in this case during the conversion

of **F** to **G** provides good circumstantial evidence that this conversion is intermolecular in nature. A similar equilibrium between a protonated species and a trifluoroacetate adduct was reported for $Os_3(CO)_9(\mu_3\text{-}\eta^2\text{-}(CH_2)_3C{=}N{-})(\mu\text{-}H)_2(CF_3COO)$ [9]. Addition of more CF_3COOH to solutions of the adduct of **9** causes no substantial changes in the NMR spectra but does result in chemical shift changes of the ^1H hydride, the aromatic hydrogen resonances , the ^{13}C carbonyl and the ^{19}F trifluoroacetate resonances. These shifts are probably due to hydrogen bonding interactions with excess acid but do not affect the interpretations presented here.

The reaction of **10** with CF_3COOH takes a distinctly different, yet simpler course than that of **9**. In presence of 1 equiv. of acid a single broad hydride resonance is observed at −14.05 ppm at room temperature. At −65 °C this broad resonance resolves into one major pair of hydride resonances at −13.94 and −14.09 ppm with very minor companion peaks at −12.18, −12.28, −13.15, −13.62, −13.67 and −14.95 ppm whose low intensities made it impossible to assign them as pairs. Similarly, the observation of one major peak at 1.35 ppm and three minor peaks at 1.61, 1.67 and 2.65 ppm in the ^{19}F NMR at −65 °C confirms that the hydride signals are due to adduct formation. Thus in the case of **10** only one isomer of the acid adduct is significantly populated at −65 °C, most likely **F**, and at room temperature the hydrides and the minor isomers are exchanging on the NMR time scale.

2.3. General conclusions

These studies have revealed some significant differences in the chemistry of **1**–**10**. First, complexes **4**–**10** have a much greater tendency to undergo addition of two electron donors than **1**–**3**. This is reflected in the larger formation constants of the amine adducts and in the formation of adducts with the weaker donors acetonitrile and trifluoroacetate. This can be rationalized by the apparent greater thermodynamic stability for the μ versus the μ_3 bonding mode for **4**–**10** relative to **1**–**3** (Fig. 2). This most likely arises from the contribution of resonance structures that make the pyridinyl nitrogen a stronger donor in the case of **5**–**10** (Scheme 2).

Second, reaction of **1**–**10** with the bulky, soft electron donor triphenylphosphine drives all the products of the resulting adducts to a common structure while the harder and less bulky ligands n-butylamine and trifluoroacetate result in a variety of isomeric adducts with a range of fluxionality and stability. Indeed, although the overall behavior of these electron deficient clusters parallels the related μ_3-imidoyl triosmium clusters the structures of some of the adducts of **1**–**10** remain in doubt for lack of solid state structural data that were available for the imidoyls [9–11,13].

Particularly puzzling, and also intriguing, are the factors governing the remarkable differences in the behavior of **5** and **7** versus **4**, **6** and **8**–**10** towards trifluoroacetic acid. We are hopeful that theoretical modeling of the bonding geometries of **1**–**10** currently underway in our laboratories will further elucidate these differences in reactivity.

The take home message of this detailed study is that subtle differences in the nature of the heterocyclic ligand can lead to dramatic differences in reactivity, even though the bonding mode of the ligand to the cluster in the entire class of molecules studied is virtually identical.

3. Experimental

3.1. Materials

Compounds **1**–**10**, **11** and **12** were synthesized by published literature procedures [4–6]. The NMR solvents $CDCl_3$, CD_2Cl_2, CD_3CN and $(CD_3)_2CO$ (Norell) were dried over molecular sieves (Type 4A, Mallincrodt). Trifluoroacetic acid (Aldrich) was distilled from P_2O_5 before use. Perfluoroboric acid (Aldrich), n-$BuNH_2$ (Aldrich) and triphenylphosphine (Strem) were used as received.

3.2. Spectra and analyses

NMR spectra were measured on a Varian Unity Plus 400 MHz Spectrometer and on a JEOL-EX 400 MHz Spectrometer. IR spectra were measured on a Perkin–Elmer 1600 and a Thermo-Nicolet 633 FT IR Spectrometers. Schwarzkopf Microanalytical Laboratories, Woodside, New York, performed elemental analyses.

3.3. Synthesis of the phosphine derivatives *13*–*15*

Compounds **4**, **5** or **10** (95 mg, 0.1 mmol) were dissolved in 20 mL CH_2Cl_2 and 26 mg (0.1 mmol) PPh_3 in 5 ml of the same solvent was slowly added to the green solution under an atmosphere of nitrogen. The solution turned from green to yellow–orange immediately. After stirring for 15 min the solution was evaporated, taken up in a minimum of CH_2Cl_2 and purified by thin layer chromatography using 20–40% CH_2Cl_2–C_6H_{14} as eluent. A single orange band was eluted yielding 110–120 mg (90–95%) of **13**–**15**.

3.4. Analytical and spectroscopic data for *13*

Anal. Calc. for $C_{35}H_{21}N_2O_9Os_3P$: C, 34.59; H, 1.74; N, 2.30. Found: C, 34.14; H, 1.90; N, 2.33%. IR (*v* CO) in CH_2Cl_2: 2091 (m), 2051 (s), 2010 (s), 1990 (s), 1931 (w) cm^{-1}. ^1H NMR (CD_2Cl_2): δ 9.21 (d, 1H), 8.45 (d,

1H), 7.85 (d, 1H), 7.35–7.15 (m, 16H), 6.9 (dd, 1H), −11.92 (d, $J^{31}P-^{1}H = 15.6$ Hz, hydride).

3.5. Analytical and spectroscopic data for **14**

Anal. Calc. for $C_{35}H_{23}N_2O_9Os_3P$: C, 34.53; H, 1.90; N, 2.30. Found: C, 35.93; H, 2.40; N, 2.05%. IR (*v* CO) in CH_2Cl_2: 2084 (m), 2040 (s), 2000 (s), 1985 (br), 1933 (w) cm^{-1}. ^1H NMR ($CDCl_3$): δ 8.83 (s, br 1H), 7.35–7.15 (m, 15H), 6.93 (d, 1H), 6.51 (m, 2H), 2.62 (s, 3H), −12.65 (d, $J^{31}P-^{1}H = 15.1$ Hz, hydride).

3.6. Analytical and spectroscopic data for **15**

Anal. Calc. for $C_{34}H_{21}NO_{10}Os_3P$: C, 33.77; H, 1.75; N, 1.15. Found: C, 33.37; H, 1.77; N, 1.00%. IR (*v* CO) in CH_2Cl_2: 2087 (m), 2048 (s), 2000 (s), 1979 (br), 1941 (w) cm^{-1}. ^1H NMR (CD_2Cl_2): δ 8.29 (s, 1H), 7.15–7.38 (m, 15H), 6.99 (d, 1H), 6.78 (d, 1H), 6.65 (dd, 1H), −13.10 (d, $J^{31}P-^{1}H = 14.4$).

3.7. Synthesis of the amine adducts **16** and **17**

Compound **2** or **5** (50 mg, ~0.05 mmol) were dissolved in 5 mL CH_2Cl_2 and 50 μl n-$BuNH_2$ (~20-fold molar excess) in 5 ml C_6H_{14} was added slowly to the solution under a nitrogen atmosphere. The dark green solution gradually turned to an amber yellow. After 1 h the solution was concentrated to half volume under a stream of nitrogen and stored at −20 °C overnight. Yellow orange crystal of the adducts precipitated (20–30 mg, 40–50% yield).

3.8. Analytical and spectroscopic data for **16**

Anal. Calc. for $C_{26}H_{20}N_2O_9Os_3$: C, 29.05; H, 1.88; N, 2.60. Found: C, 29.66; H, 2.20; N, 3.13%. IR (*v* CO) in CH_2Cl_2: 2097 (w), 2073 (w), 2018 (s, br), 1972 (m), 1935 (s, br) cm^{-1}. ^1H NMR ($CDCl_3$, major isomer only): δ 9.10 (s, 1H), 8.60 (d, 1H), 8.27 (d, 1H), 8.10 (d, 1H), 7.99 (d, 1H), 7.85 (dd, 1H), 7.67 (dd, 1H), 7.31 (d, 1H), 6.78 (br, 2H), 4.58 (m, br, 1H), 4.04 (m, br), 3.40 (m, br, 2H), 2.88 (t, br, 3H), 2.76 (m, br, 2H), −13.23 (s, br, hydride).

3.9. Analytical and spectroscopic data for **17**

Anal. Calc. for $C_{21}H_{18}N_3O_9Os_3$: C, 24.54; H, 1.85; N, 4.09. Found: C, 25.16; H, 2.22; N, 4.18%. IR (*v* CO) in CH_2Cl_2: cm^{-1}. ^1H NMR (CD_2Cl_2, major isomer only): δ 9.45 (s, br, 1H), 7.65 (dd, 1H), 6.94 (m, 2H), 2.75 (s, 3H), 2.12 (m, 2H), 1.56 (s, br, 2H), 1.38 (m, 2H), 0.89 (m, 2H), 0.56 (t, 3H), 0.25 (m, 2H), −11.78 (s, hydride).

3.9.1. Measurement of the formation constants for the amine adducts

Compounds **1**–**10** (20–30 mg) was weighed directly into an NMR tube and 0.75 mL of $CDCl_3$, CD_2Cl_2 or $(CD_3)_2CO$ were added by syringe. A 10–20-fold molar excess of n-$BuNH_2$ (25–50 μL) was added slowly by syringe, the tube was shaken vigorously and the ^1H NMR were measured immediately, 5 h later and after 24 h. Equilibrium constants were calculated from the relative intensity of the hydride ^1H NMR signals and the known concentrations of **1**–**10** and n-$BuNH_2$.

3.10. Crystal structure analysis of **16**

A suitable crystal of **16**, obtained by crystallization from a CH_2Cl_2 solution containing an excess of n-$BuNH_2$, was mounted on a glass fiber using superglue. The crystal was placed in a nitrogen gas stream at 110 K on a Bruker D8 SMART APEX CCD sealed tube diffractometer with graphite monochromated Mo Kα radiation. A sphere of data was measured using a series of combinations of ϕ- and ω-scans with 10 s frame exposures and 0.3° frame widths. Data collection indexing and initial cell refinements were all handled using SMART [14] software. Frame integration and final cell refinements were carried out using SAINT [15] software. The final cell parameters were determined from least-squares refinement on a maximum of 9999 reflections. The SADABS [16] was used to carry out absorption corrections.

The structure was solved using direct methods and difference Fourier techniques (SHELXTL, V5.10) [17]. Hydrogen atoms were placed in their expected chemical positions using the HFIX command and were included in the final cycles of least-squares with isotropic U_{ij}'s related to the atoms ridden upon. The C–H distances were fixed at 0.93, 0.98 (CH_4), 0.97 (methylene), or 0.96 Å (methyl). The position of the hydride was calculated using the program HYDEX [12]. All non-hydrogen atoms were refined anisotropically except for the n-$BuNH_2$ ligand atoms. Scattering factors and anomalous dispersion corrections are taken from the *International Tables for X-ray Crystallography* [18]. Structure, solution refinement, graphics and generation of publication materials were performed using SHELXTL, V5.10 [17] software. Additional details of data collection and structure refinement are given in Table 4.

4. Supplementary material

Crystallographic data for the structural analysis have been deposited with the Cambridge Crystallographic Data Centre, CCDC No. 158306 for compound **16**. Copies of this information may be obtained free of charge from The Director, CCDC, 12 Union Road,

Cambridge, CB2 1EZ, UK (fax: +44-1223-336-033; e-mail: deposit@ccdc.cam.ac.uk or www: http://www.ccdc.cam.ac.uk).

Acknowledgements

We gratefully acknowledge the support of the National Science Foundation (E.R., CHE-9625367), The University of Torino (E.R. and L.M.). Financial support from MURST and CNR (L.M. and R.B.) is also gratefully acknowledged.

References

[1] E. Rosenberg, S.E. Kabir, D. Kolwaite, K.I. Hardcastle, W. Crosswell, J. Grindstaff, Organometallics 14 (1995) 3611.
[2] E. Rosenberg, E. Arcia, D.S. Kolwaite, K.I. Hardcastle, J. Ciurash, R. Duque, R. Gobetto, L. Milone, D. Osella, M. Botta, W. Dastrù, A. Viale, J. Fiedler, Organometallics 17 (1998) 415.
[3] E. Rosenberg, B. Bergman, A. Bar Din, R. Smith, R. Gobetto, L. Milone, A. Viale, W. Dastru', Polyhedron 17 (1998) 2975.
[4] B. Bergman, R.H. Holmquist, R. Smith, E. Rosenberg, K.I. Hardcastle, M. Visi, J. Ciurash, J. Am. Chem. Soc. 120 (1998) 12818.
[5] J. Abedin, B. Bergman, R. Holmquist, R. Smith, E. Rosenberg, J. Ciurash, K. Hardcastle, J. Roe, V. Vazquez, C. Roe, S. Kabir, B. Roy, S. Alam, K.A. Azam, Coord. Chem. Rev. 190–192 (1999) 975.
[6] R. Smith, E. Rosenberg, K.I. Hardcastle, V. Vazquez, J. Roh, Organometallics 18 (1999) 3519.
[7] S.T. Beatty, B. Bergman, E. Rosenberg, W. Dastru', R. Gobetto, L. Milone, A. Viale, J. Organomet. Chem. 593–594 (1999) 226.
[8] E. Rosenberg, L. Milone, C. Nervi, D. Osella, J. Fiedler, Md.J. Abedin, D. Rokhsana, Inorg. Chim. Acta 300 (2000) 766.
[9] E. Rosenberg, K.I. Hardcastle, S.E. Kabir, L. Milone, R. Gobetto, M. Botta, N. Nishimura, M. Yin, Organometallics 14 (1995) 3068.
[10] E. Rosenberg, S.E. Kabir, M. Day, K.I. Hardcastle, E. Wolf, T. McPhillips, Organometallics 14 (1995) 721.
[11] E. Rosenberg, D. Espitia, S.E. Kabir, T. McPhillips, M.W. Day, K.I. Hardcastle, R. Gobetto, D. Osella, L. Milone, Organometallics 10 (1991) 3550.
[12] A.G. Orpen, J. Chem. Soc., Dalton. Trans. (1980) 2509.
[13] E. Rosenberg, S.E. Kabir, M. Day, K.I. Hardcastle, Organometallics 13 (1994) 4437.
[14] SMART Version 5.55, Bruker AXS Inc., Analytical X-ray Systems, Madison, WI, 2000.
[15] SAINT version 6.02, Bruker AXS Inc., Analytical X-ray Systems, Madison, WI, 1999.
[16] SADABS, George Sheldrick, University of Göttingen, Göttingen, Germany, 1996.
[17] SHELXTL V5.10, Bruker AXS Inc., Analytical X-ray Systems, Madison, WI, 1997.
[18] A.J.C. Wilson (Ed.), International Tables of X-ray Crystallography, vol. C, Kluwer Academic, Dordrecht, 1992, Tables 6.1.1.4 (pp. 500–5020) and 4.2.6.8 (pp. 219–222).